

Radiative corrections to the lepton current in unpolarized elastic lp -interaction for fixed Q^2 and scattering angle

A. Afanasev^{a,1}, A. Ilyichev^{b,2,3}

¹Department of Physics, The George Washington University, Washington, DC 20052 USA

²Belarusian State University, 220030 Minsk, Belarus

³Institute for Nuclear Problems, Belarusian State University, 220006 Minsk, Belarus

Received: date / Accepted: date

Abstract The kinematical difference between the description of radiative effects for fixed Q^2 vs a fixed scattering angle in the elastic lepton-proton (lp)-scattering is discussed. The technique of calculation as well as explicit expressions for radiative corrections to the lepton current in unpolarized elastic lp -scattering for these two cases are presented without using an ultrarelativistic approximation. A comparative numerical analysis within kinematic conditions of Jefferson Lab measurements and MUSE experiment in PSI is performed.

1 Introduction

The elastic lepton-proton scattering is a recognized tool for investigation of the internal proton structure. The observation of the disagreement in Q^2 -behavior of the proton elastic form factor ratio for unpolarized [1, 2] and polarized [3, 4] electron scattering, along with the proton radius puzzle coming from the different outcomes of the measurements in electron-proton systems [5, 6] and in the muonic hydrogen [7] – all of these require understanding of underlying QED processes that may lead to systematic uncertainties at a per cent level. Moreover, the results of the recent experiment PRAD [8] was in agreement with muonium spectroscopy experiment that contradicted the previous electron-proton scattering data. This unexpected result motivates new efforts for the theoretical and experimental investigations.

One of the important and essential tools for the investigation of the electromagnetic properties of the proton is an experimental program with high duty-cycle positron beams at JLab [9]. This program with the electron beams allows to estimate the electromagnetic form

factors of the proton separately as well as to measure a charge asymmetry that appears at the lowest order as an interference of the matrix elements with one- and two-photon exchanges.

Together with widely discussed two-photon exchange [10], the important source of uncertainties for both lepton and anti-lepton scattering is from the real photon emission accompanying any process with the charge particle scattering, as well as the additional virtual particle contributions. Due to smallness of muon beam momentum at MUSE experiment in PSI [11], as well as scattering by extremely small angles in PRAD-II experiment at Jefferson Lab [12], all calculations have to be performed beyond the ultrarelativistic approximation, *i.e.* retaining lepton's mass during the entire calculation. While for purely elastic scattering at a given beam energy the four-momentum transfer Q^2 is in one-to-one correspondence with a lepton scattering angle, this is not the case for radiative events. It is therefore of critical importance to understand the role of QED radiative corrections (RC) in different kinematic scenarios: fixed momentum transfer Q^2 vs fixed scattering angle of the detected lepton (as done in MUSE [11] or in high-resolution spectrometers with small angular acceptance used in some of Jefferson Lab experiments).

It should be noted that rather often for estimation of the similar corrections to the exclusive process the additional particle contributions are calculated exactly or within ultrarelativistic approximation (with respect to lepton's mass) while the real photon emission is considered within the soft photon approximation. Particularly in the papers [13] and [14] for Möller and virtual Compton scattering processes, respectively, the virtual QED corrections have been calculated beyond the ultrarelativistic limit but only the soft part of the real photon emission was taken into account.

^ae-mail: afanas@gwu.edu

^be-mail: ily@hep.by

Mo and Tsai first developed a systemic approach to calculate RC with hard photon emission in elastic and inelastic electron-proton scattering [15]. One limitation in their calculations was the approximate way to consider the soft-photon contribution, as a result, their final expressions depend on an artificial parameter Δ that was introduced to separate the photon momentum phase space into soft and hard parts.

Here we present the explicit expressions as well as the numerical comparison of RC to the lepton current both for fixed scattering angle and transferred momentum squared. Such RC include hard real photon emission from the initial and final leptons, vacuum polarization and vertex correction. The presented RC are charge-even, therefore they directly apply to a sum of positron- and electron scattering cross sections that could be measured by combined experiments with added positron capabilities at JLab.

For extraction and cancellation of the infrared divergence we use the covariant approach of Bardin-Shumeiko [16]. One of the important advantages of this approach over [15] consists in the independence of the final results from the parameter Δ . A similar calculation but for fixed transferred momentum squared was performed in Ref. [17].

Among the other recent results on RC calculations to the lepton current with the hard photon emission and keeping the lepton mass, we specifically mention two papers. The first one is by Bucoveanu and Spiesberger [18] and includes the second-order RC. The second publication describes FORTRAN code developed by Banerjee, Engel, Signer, and Ulrich [19] with a calculation of the first order RC to several processes in elastic lepton-lepton and lepton-proton scattering.

The rest of the article is organized as follows. The kinematics of elastic process and radiative process are discussed in detail in Sec. 2. In particular, we show that for the description of hard photon emission at fixed scattering angle the ultrarelativistic approximation is not applicable even for relativistic electron-proton scattering. The hadronic tensor and Born cross section are presented in Sec. 3. The additional virtual particle contributions are given in Sec. 4. For the parameterization of the infrared and ultraviolet divergences the dimensional regularization is used. In the next two sections the real photon emission contribution for both fixed Q^2 and fixed scattering angle is presented. For both cases the infrared divergence is extracted and cancelled using the Bardin-Shumeiko approach [16]. The comparative numerical analysis for MUSE [11] and [20,21] experiments can be found in Sec. 7. A brief discussion and conclusions are presented in the last section. The details of the approach for the infrared divergence extraction

are given in Appendix A. The derivation of the compact expression for the Bardin-Shumeiko function S_ϕ can be found in Appendix B.

2 Elastic and inelastic processes

The unpolarized elastic lp -scattering

$$l(k_1) + p(p_1) \rightarrow l'(k_2) + p'(p_2), \quad (1)$$

is considered first. Here k_1 and p_1 (k_2 and p_2) are the four-momenta of the initial (final) lepton and proton respectively ($k_1^2 = k_2^2 = m^2$, $p_1^2 = p_2^2 = M^2$). Although we consider this process in the target rest frame ($\mathbf{p}_1 = 0$), after definition of the virtual photon momentum as $q = k_1 - k_2$, it will be useful to introduce the kinematic invariants:

$$\begin{aligned} S &= 2p_1 k_1, \quad Q^2 = -q^2, \quad X = S - Q^2, \\ \lambda_S &= S^2 - 4m^2 M^2, \quad \lambda_X = X^2 - 4m^2 M^2, \\ \lambda_m &= Q^2(Q^2 + 4m^2), \end{aligned} \quad (2)$$

in such a way, that the energies of the initial (k_{10}) and final (k_{20}) leptons as well as the absolute value of their three-momenta ($|\mathbf{k}_1|$ and $|\mathbf{k}_2|$, respectively) read:

$$k_{10} = \frac{S}{2M}, \quad |\mathbf{k}_1| = \frac{\sqrt{\lambda_S}}{2M}, \quad k_{20} = \frac{X}{2M}, \quad |\mathbf{k}_2| = \frac{\sqrt{\lambda_X}}{2M}. \quad (3)$$

In the present paper we will consider two types of the cross sections: $d\sigma/dQ^2$ and $d\sigma/d\cos\theta$ where the cosine of the scattering angle θ can be expressed through the invariants:

$$\cos\theta = \frac{\mathbf{k}_1 \cdot \mathbf{k}_2}{|\mathbf{k}_1||\mathbf{k}_2|} = \frac{SX - 2M^2(Q^2 + 2m^2)}{\sqrt{\lambda_S \lambda_X}}. \quad (4)$$

Taking into account $X = S - Q^2$, the quadratic equation over Q^2 has two solutions

$$Q_\pm^2 = \lambda_S \frac{S \sin^2\theta + 2M^2 \pm 2M \cos\theta \sqrt{M^2 - m^2 \sin^2\theta}}{(S + 2M^2)^2 - \lambda_S \cos^2\theta}, \quad (5)$$

where the direct substitution into (4) shows that Q_-^2 is the correct expression while Q_+^2 corresponds to the scattering on $180^\circ - \theta$ angle:

$$\frac{S(S - Q_\pm^2) - 2M^2(Q_\pm^2 + 2m^2)}{\sqrt{\lambda_S((S - Q_\pm^2)^2 - 4m^2 M^2)}} = \mp \cos\theta. \quad (6)$$

The restrictions on the scattering angle $-1 < \cos\theta < 1$ translate into the kinematical limits for Q^2 :

$$0 < Q^2 < \frac{\lambda_S}{S + m^2 + M^2}. \quad (7)$$

For the description of the inelastic process caused by real photon emission

$$l(k_1) + p(p_1) \rightarrow l'(k_2) + p'(p_2) + \gamma(k) \quad (8)$$

($k^2 = 0$) three additional variables have to be introduced. We choose the standard set [22] of them: inelasticity $v = (p_1 + k_1 - k_2)^2 - M^2$, $\tau = kq/kp_1$ and the azimuthal angle ϕ_k between $(\mathbf{k}_1, \mathbf{k}_2)$ and (\mathbf{k}, \mathbf{q}) planes in the rest frame ($\mathbf{p}_1 = 0$).

Using this set of variables, it is straightforward to show that for real photon emission the expressions for the energy and the three-momentum of the scattering lepton have to be modified:

$$k_{20} = \frac{X - v}{2M}, \quad |\mathbf{k}_2| = \frac{\sqrt{(X - v)^2 - 4m^2M^2}}{2M}. \quad (9)$$

As a result, $\cos \theta$ can be expressed through the inelasticity value and Q^2 in a following way:

$$\cos \theta_R = \frac{S(X - v) - 2M^2(Q^2 + 2m^2)}{\sqrt{\lambda_S((X - v)^2 - 4M^2m^2)}}, \quad (10)$$

where we introduce the index R to emphasize that at a fixed Q^2 the value of $\cos \theta$ depends on the inelasticity of the radiative process. The restrictions on the scattering angle $-1 < \cos \theta_R < 1$ set the upper limit for v at fixed Q^2 :

$$v_q = \frac{\sqrt{\lambda_S} \sqrt{\lambda_m} - Q^2(S + 2m^2)}{2m^2}. \quad (11)$$

Similar to the non-radiative process, there are two possible ways to express Q^2 from Eq. (10). After substitution of the obtained expressions for Q^2 into the r.h.s. of Eq. (10), the correct solution here is:

$$Q_R^2(v) = \frac{1}{(S + 2M^2)^2 - \lambda_S \cos^2 \theta} \times \left[(S + 2M^2)(\lambda_S - vS) - \lambda_S(S - v) \cos^2 \theta - 2M \sqrt{\lambda_S} \sqrt{D} \cos \theta \right], \quad (12)$$

where the index R poses the same meaning as in Eq. (10), namely, at a fixed $\cos \theta$ the value of Q^2 depends on the inelasticity of the radiative process. The quantity

$$D = M^2(\lambda_S + v(v - 2S)) - m^2(\lambda_S \sin^2 \theta + 4vM^2) \quad (13)$$

must be positive. It turns out that the upper limit of v for a given scattering angle follows from that restriction:

$$v_\theta = S + 2m^2 - \frac{m}{M} \sqrt{(S + 2M^2)^2 - \lambda_S \cos^2 \theta}. \quad (14)$$

Notice that minimizing D maximizes Q_R^2 if $\cos \theta > 0$ and minimizes Q_R^2 if $\cos \theta < 0$. The energy and momentum of the scattering lepton for fixed angle read:

$$k_{20} = \frac{S - Q_R^2(v) - v}{2M}, \quad |\mathbf{k}_2| = \frac{\lambda_S - vS - Q_R^2(v)(S + 2M^2)}{2M \cos \theta \sqrt{\lambda_S}}. \quad (15)$$

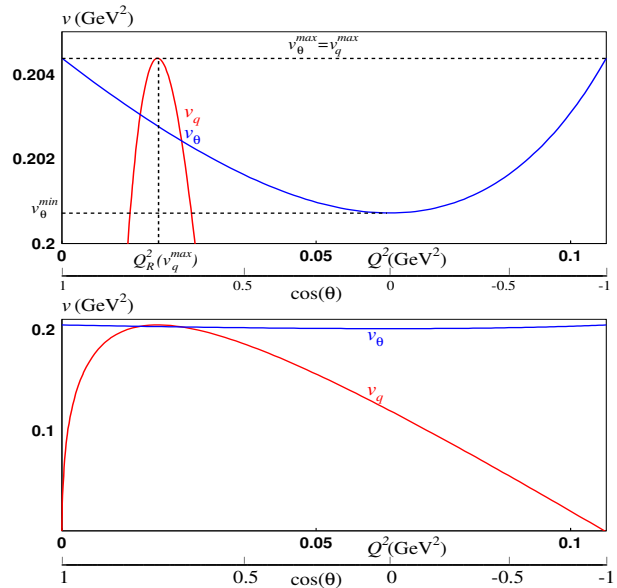


Fig. 1 The dependence of the upper inelasticity limits v_q and v_θ on the observable variables for the muon beam momentum $|\mathbf{k}_1| = 200$ MeV. Lowest: a full kinematic range. Upper: a close-up of the region near the kinematic boundary. The quantities $v_\theta^{max} = v_q^{max}$, v_θ^{min} and $Q_R^2(v_q^{max})$ are defined by Eqs. (16), (18) and (17) respectively.

From Fig. 1 one can see that when the observable quantity Q^2 is close to its kinematical boundaries, the allowed range of the inelasticity reduces to zero that makes it impossible to emit any real photon. The maximum value of the inelasticity

$$v_q^{max} = S - 2m(\sqrt{S + m^2 + M^2} - m) \quad (16)$$

comes at the point that can be obtained after substitution (16) into (12),

$$Q_R^2(v_q^{max}) = \frac{m(S + 2m^2)}{\sqrt{S + m^2 + M^2}} - 2m^2. \quad (17)$$

From the upper plot of Fig. 1 we can see that for fixed angle the upper inelasticity limit reaches its maximum value $v_\theta^{max} = v_q^{max}$ at the kinematical boundaries $\cos \theta = \pm 1$ and has a minimum

$$v_\theta^{min} = (S - 2mM) \left(1 - \frac{m}{M}\right) \quad (18)$$

at $\cos \theta = 0$.

The dependence of Q_R^2 on the inelasticity at different fixed angles is presented in Fig. 2. From this plot one can see that even for $\theta = 0^\circ$ real photon emission is not prohibited by any kinematical restrictions. Opposite to the elastic process, the scattering under zero angle induces non-zero transferred momentum.

After substitution of (14) into (12) we find the line with boundary common points for θ and $180^\circ - \theta$ curves

$$Q_R^2(v_\theta) = \frac{m(S(S + 2M^2) - \lambda_S \cos^2 \theta)}{M \sqrt{(S + 2M^2)^2 - \lambda_S \cos^2 \theta}} - 2m^2 \quad (19)$$

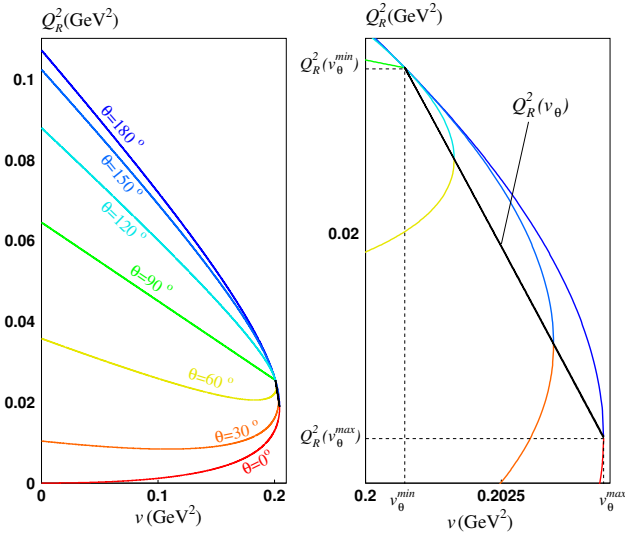


Fig. 2 The dependence of Q_R^2 on v , as given by Eq. (12) for the different fixed scattering angles and the muon beam momentum $|\mathbf{k}_1| = 200$ MeV. Left: a full kinematic range. Right: a close-up of the region near the kinematic boundary. The joining curves θ and $180^\circ - \theta$ line describes by Eq. (19). The two indicated points are $(v_\theta^{min}, Q_R^2(v_\theta^{min}))$ according to Eqs. (18) and (20), and $(v_\theta^{max}, Q_R^2(v_\theta^{max}))$ according to Eqs. (16) and (17).

as it is presented in the right plot of Fig. 2. The quantity $Q_R^2(v_\theta^{max})$ is defined by Eq. (17) while

$$Q_R^2(v_\theta^{min}) = m \left(\frac{S}{M} - 2m \right). \quad (20)$$

From Eq. (19) it can be seen that for the description of hard photon emission at fixed scattering angle even for high-energy electron-proton scattering the ultrarelativistic approximation is not applicable.

In practice, however, the contribution of the hard real photon emission to the cross section can be essentially reduced by applying a cut v_{cut} on the inelasticity which is also a measured quantity in the single-arm measurement of the elastically scattered lepton only. Therefore, keeping in mind the inelasticity maximum values, for an upper limit of this quantity both for the fixed Q^2 and scattering angle we will use v_{cut} as an experimentally observable variable.

The other invariant quantity τ can be calculated in the rest frame as

$$\tau = \frac{1}{M} (q_0 - |\mathbf{q}| \cos \theta_k), \quad (21)$$

where q_0 (\mathbf{q}) is the energy (three-momentum) of the transfer momentum q and θ_k is the polar angle between the three-momenta \mathbf{q} and \mathbf{k} . The range of this variable is defined through $-1 < \cos \theta_k < 1$ and for fixed Q^2 and fixed angle θ it reads:

$$\tau_{max/min}^q = \frac{Q^2 + v \pm \sqrt{\lambda_q}}{2M^2},$$

$$\tau_{max/min}^\theta = \frac{Q_R^2(v) + v \pm \sqrt{\lambda_v}}{2M^2} \quad (22)$$

with $\lambda_q = (Q^2 + v)^2 + 4M^2Q^2$ and $\lambda_v = (Q_R^2(v) + v)^2 + 4M^2Q_R^2(v)$.

At the end of this Section it is necessary to say about the orientation of the azimuthal photon angle ϕ_k . It can be defined by choosing a sing in the expression of $\sin \phi_k$ through the pseudoscalar quantity as

$$\sin \phi_k = \pm \frac{\varepsilon_{\alpha\beta\gamma\delta} p_1^\alpha q^\beta k_1^\gamma k^\delta}{M |\mathbf{q}| |\mathbf{k}_1^\perp| k_0 \sin \theta_k}, \quad (23)$$

where \mathbf{k}_1^\perp is the transverse three-momenta of the incoming or scattering lepton with respect to \mathbf{q} , k_0 is a photon energy. However, during the estimation of the real photon contribution to elastic or inclusive lepton-proton scattering even for polarized particles in contrast to the exclusive or semi-inclusive hadron lepton-production the sine of ϕ_k does not appear for any stage of calculations. Therefore, we are not concerned about this problem and integrate over ϕ_k without taking into account its orientation.

3 Hadronic tensor and Born contribution

Born contribution to the process depicted by the Feynman graph in Fig. 3(a) reads:

$$d\sigma_B = \frac{1}{2\sqrt{\lambda_S}} \mathcal{M}_B^2 d\Gamma_2, \quad (24)$$

where the phase space has the form

$$\begin{aligned} d\Gamma_2 &= \frac{1}{(2\pi)^2} \delta^4(p_1 + k_1 - p_2 - k_2) \frac{d^3 k_2}{2k_{20}} \frac{d^3 p_2}{2p_{20}} \\ &= \frac{dQ^2}{8\pi\sqrt{\lambda_S}} = \frac{\sqrt{\lambda_X} d\cos\theta}{8\pi(S + 2M^2 - \cos\theta X \sqrt{\lambda_S/\lambda_X})}. \end{aligned} \quad (25)$$

The matrix element squared is expressed through the convolution of the leptonic and hadronic tensors

$$\mathcal{M}_B^2 = \frac{e^4}{Q^4} W_{\mu\nu}(q) L^{\mu\nu}. \quad (26)$$

The leptonic tensor is well known:

$$L_B^{\mu\nu} = \frac{1}{2} \text{Tr}[\gamma^\mu (\hat{k}_1 + m) \gamma^\nu (\hat{k}_2 + m)], \quad (27)$$

while the hadronic tensor can be defined through the on-shell proton vertex

$$\Gamma_\mu(q) = \gamma_\mu F_d(-q^2) + \frac{i\sigma_{\mu\nu} q^\nu}{2M} F_p(-q^2), \quad (28)$$

where $F_d(F_p)$ is Dirac (Pauli) form factor, in the following way

$$W_{\mu\nu}(q) = \frac{1}{2} \text{Tr}[\Gamma_\mu(q)(\hat{p}_1 + M)\Gamma_\nu(-q)(\hat{p}_1 + \hat{q} + M)] \quad (29)$$

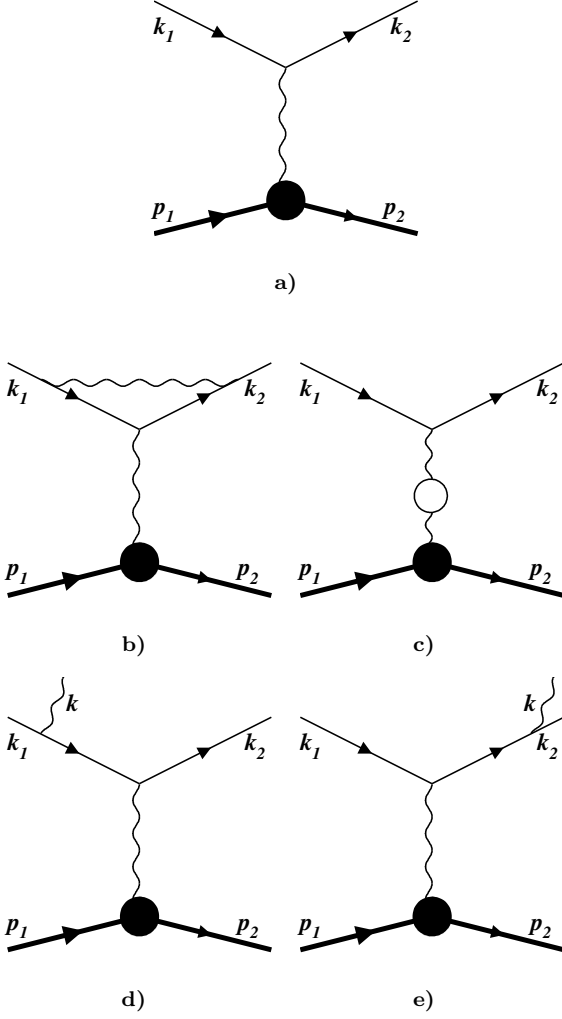


Fig. 3 Feynman graphs corresponding to the Born contribution (a), leptonic vertex correction (b), vacuum polarization (c), and real photon emission from initial (d) and final (e) leptons.

and then rearranged into covariant form

$$\begin{aligned}
 W_{\mu\nu}(q) &= -\left(g_{\mu\nu} - \frac{q_\mu q_\nu}{q^2}\right) \mathcal{F}_1(-q^2) \\
 &\quad + \left(p_{1\mu} + \frac{q_\mu}{2}\right) \left(p_{1\nu} + \frac{q_\nu}{2}\right) \frac{\mathcal{F}_2(-q^2)}{2M^2} \\
 &= \sum_{i=1}^2 w_{\mu\nu}^i(q) \mathcal{F}_i(-q^2).
 \end{aligned} \tag{30}$$

Here

$$\begin{aligned}
 \mathcal{F}_1(-q^2) &= -q^2(F_d(-q^2) + F_p(-q^2))^2, \\
 \mathcal{F}_2(-q^2) &= 4M^2 F_d(-q^2)^2 - q^2 F_p(-q^2)^2.
 \end{aligned} \tag{31}$$

As a result, after convolution we have

$$\frac{d\sigma_B}{dQ^2} = \frac{2\pi\alpha^2}{\lambda_S Q^4} \sum_{i=1}^2 \theta_B^i \mathcal{F}_i(Q^2),$$

$$\frac{d\sigma_B}{d\cos\theta} = j_\theta \frac{d\sigma_B}{dQ^2}, \tag{32}$$

where

$$j_\theta = \frac{\sqrt{\lambda_S} \lambda_X^{3/2}}{2M^2(SX - 2m^2(Q^2 + 2M^2))}, \tag{33}$$

and

$$\theta_B^1 = Q^2 - 2m^2, \quad \theta_B^2 = \frac{SX - M^2 Q^2}{2M^2}. \tag{34}$$

4 Additional virtual particle contribution

The additional virtual particle contribution can be expressed through Eqs. (24,26) with replacement of the leptonic tensor (27) by

$$\begin{aligned}
 L_V^{\mu\nu} &= \frac{1}{2} \text{Tr}[(\hat{k}_2 + m) \Gamma_V^\mu (\hat{k}_1 + m) \gamma^\nu] \\
 &\quad + \frac{1}{2} \text{Tr}[(\hat{k}_2 + m) \gamma^\mu (\hat{k}_1 + m) \bar{\Gamma}_V^\nu],
 \end{aligned} \tag{35}$$

where the leptonic vertex Γ_V contains the sum of both the lepton vertex correction Λ^μ and vacuum polarization by lepton $\Pi_\alpha^{l\mu}$ represented by the Feynman graphs in Fig. 3(b) and Fig. 3(c), respectively

$$\begin{aligned}
 \Gamma_V^\mu &= \Lambda^\mu + \Pi_\alpha^{l\mu} \gamma^\alpha, \\
 \bar{\Gamma}_V^\nu &= \gamma_0 \Gamma_V^{\nu\dagger} \gamma_0.
 \end{aligned} \tag{36}$$

Similar to [17] we do not consider the vacuum polarization by the hadron.

Since Λ_μ and $\Pi_\alpha^{l\mu}$ contain the ultraviolet divergence while Λ_μ also includes the infrared divergent terms, both of these contributions have to be calculated analytically, and we choose dimensional regularization for this calculation.

After the analytical calculation – detail of which can be found in Appendix D of [23] – Λ_μ and $\Pi_{\alpha\mu}^i$ read:

$$\begin{aligned}
 \Lambda_\mu &= \frac{\alpha}{2\pi} \left(\delta_{\text{vert}}^{UV}(Q^2) \gamma_\mu - \frac{1}{2} m L_m [\hat{q}, \gamma_\mu] \right), \\
 \Pi_{\alpha\mu}^l &= \frac{\alpha}{2\pi} \left(g_{\alpha\mu} + \frac{q_\alpha q_\mu}{Q^2} \right) \sum_{i=e,\mu,\tau} \delta_{\text{vac}}^{iUV}(Q^2).
 \end{aligned} \tag{37}$$

The term in Λ_μ proportional to

$$L_m = \frac{1}{\sqrt{\lambda_m}} \log \frac{\sqrt{\lambda_m} + Q^2}{\sqrt{\lambda_m} - Q^2} \tag{38}$$

is the anomalous magnetic moment whose contribution reads

$$\begin{aligned}
 \frac{d\sigma_{AMM}}{dQ^2} &= \frac{\alpha^3 m^2 L_m}{2M^2 Q^2 \lambda_S} \\
 &\quad \times \left[12M^2 \mathcal{F}_1(Q^2) - (Q^2 + 4M^2) \mathcal{F}_2(Q^2) \right], \\
 \frac{d\sigma_{AMM}}{d\cos\theta} &= j_\theta \frac{d\sigma_{AMM}}{dQ^2}.
 \end{aligned} \tag{39}$$

The ultraviolet divergence contained in the remaining terms of Eqs (37) can be removed by applying the mass-shell renormalization procedure that requires their vanishing at $Q^2 \rightarrow 0$:

$$\begin{aligned}\delta_{\text{vert}} &= \delta_{\text{vert}}^{UV}(Q^2) - \delta_{\text{vert}}^{UV}(0), \\ \delta_{\text{vac}}^i &= \delta_{\text{vac}}^{iUV}(Q^2) - \delta_{\text{vac}}^{iUV}(0).\end{aligned}\quad (40)$$

As a result, we obtain

$$\begin{aligned}\delta_{\text{vert}} &= -J_0 \left(P_{IR} + \log \frac{m}{\mu} \right) - 2 + \left(\frac{3}{2} Q^2 + 4m^2 \right) L_m \\ &\quad - \frac{Q^2 + 2m^2}{\sqrt{\lambda_m}} \left(\frac{1}{2} \lambda_m L_m^2 + 2\text{Li}_2 \left[\frac{2\sqrt{\lambda_m}}{Q^2 + \sqrt{\lambda_m}} \right] \right. \\ &\quad \left. - \frac{\pi^2}{2} \right), \\ \delta_{\text{vac}}^l &= \sum_{i=e,\mu,\tau} \delta_{\text{vac}}^i = \sum_{i=e,\mu,\tau} \left[\frac{2}{3} (Q^2 + 2m_i^2) L_m^i \right. \\ &\quad \left. - \frac{10}{9} + \frac{8m_i^2}{3Q^2} (1 - 2m_i^2 L_m^i) \right].\end{aligned}\quad (41)$$

Here

$$J_0 = 2((Q^2 + 2m^2)L_m - 1), \quad (42)$$

μ is an arbitrary parameter of the dimension of a mass,

$$P_{IR} = \frac{1}{n-4} + \frac{1}{2} \gamma_E + \log \frac{1}{2\sqrt{\pi}} \quad (43)$$

is the infrared divergent term,

$$\text{Li}_2(x) = - \int_0^x \frac{\log|1-y|}{y} dy \quad (44)$$

is Spence's dilogarithm, and

$$L_m^i = \frac{1}{\sqrt{\lambda_m^i}} \log \frac{\sqrt{\lambda_m^i} + Q^2}{\sqrt{\lambda_m^i} - Q^2}, \quad \lambda_m^i = Q^2(Q^2 + 4m_i^2). \quad (45)$$

Finally, the virtual particle contribution reads

$$\frac{d\sigma_V}{d\zeta} = \frac{d\sigma_{AMM}}{d\zeta} + \frac{\alpha}{\pi} (\delta_{\text{vert}} + \delta_{\text{vac}}^l) \frac{d\sigma_B}{d\zeta}, \quad (46)$$

where $\zeta = Q^2$ or $\cos\theta$.

It should be noted that the above obtained expressions for the virtual particle contributions agree with the results given in Section 3 of [13] and in Appendix A of [14]. Particularly, while the comparison with [14] is straightforward, to verify agreement of our results with [13] we present Eq. (46) in the electron-muon scattering limit: $F_d \rightarrow 1$, $F_p \rightarrow 0$, $M \rightarrow m_\mu$ and $m \rightarrow m_e$.

5 Real photon emission for fixed Q^2

The contribution of real photon emission from the lepton leg presented in Fig. 3(d, e) has a form:

$$d\sigma_R = \frac{1}{2\sqrt{\lambda_S}} \mathcal{M}_R^2 d\Gamma_3, \quad (47)$$

where the phase space can be expressed through the photonic variables introduced after (8)

$$\begin{aligned}d\Gamma_3 &= \frac{1}{(2\pi)^5} \delta^4(p_1 + k_1 - p_2 - k_2 - k) \frac{d^3k}{2k_0} \frac{d^3k_2}{2k_{20}} \frac{d^3p_2}{2p_{20}} \\ &= \frac{dQ^2 v dv d\tau d\phi_k}{2^8 \pi^4 (1+\tau)^2 \sqrt{\lambda_S \lambda_q}}.\end{aligned}\quad (48)$$

The matrix element squared reads

$$\mathcal{M}_R^2 = \frac{e^6}{t^2} W_{\mu\nu}(q-k) L_R^{\mu\nu}, \quad (49)$$

where $t = -(q-k)^2 = Q^2 + \tau R$ and $R = 2p_1 k = v/(1+\tau)$. The leptonic tensor reads:

$$L_R^{\mu\nu} = -\frac{1}{2} \text{Tr}[\Gamma_R^{\mu\alpha}(\hat{k}_1 + m) \bar{\Gamma}_{R\alpha}^\nu(\hat{k}_2 + m)], \quad (50)$$

with

$$\begin{aligned}\Gamma_R^{\mu\alpha} &= \left(\frac{k_1^\alpha}{k k_1} - \frac{k_2^\alpha}{k k_2} \right) \gamma^\mu - \frac{\gamma^\mu \hat{k} \gamma^\alpha}{2k k_1} - \frac{\gamma^\alpha \hat{k} \gamma^\mu}{2k k_2}, \\ \Gamma_{R\alpha}^\nu &= \left(\frac{k_{1\alpha}}{k k_1} - \frac{k_{2\alpha}}{k k_2} \right) \gamma^\nu - \frac{\gamma^\nu \hat{k} \gamma_\alpha}{2k k_2} - \frac{\gamma_\alpha \hat{k} \gamma^\nu}{2k k_1}.\end{aligned}\quad (51)$$

It is convenient to introduce the following convolutions integrated over ϕ_k :

$$\begin{aligned}\int_0^{2\pi} d\phi_k L_R^{\mu\nu} w_{\mu\nu}^i(q-k) &= -4\pi \sqrt{\lambda_q} \sum_{j=1}^{k_i} R^{j-3} \\ &\quad \times \theta_{ij}(v, \tau, Q^2).\end{aligned}\quad (52)$$

Here $k_i = \{3, 4\}$, $\theta_{i1}(v, \tau, Q^2) = 4\theta_B^i F_{IR}$ and the other components of $\theta_{ij}(v, \tau, Q^2)$ tensor read:

$$\begin{aligned}\theta_{12} &= 4\tau F_{IR}, \\ \theta_{13} &= -4F - 2\tau^2 F_d, \\ \theta_{22} &= \frac{1}{2M^2} \left[2(Q^2 - 2\tau M^2 - 2(1+\tau)S) F_{IR} \right. \\ &\quad \left. + S_p(Q^2 F_{1+} + 2F_{2-} - \tau S_p F_d) \right], \\ \theta_{23} &= \frac{1}{2M^2} \left[(\tau(2\tau M^2 - Q^2) + 4m^2) F_d - S_p F_{1+} \right. \\ &\quad \left. + 2(1+\tau)(\tau S_p F_d + X F_{1+} + F_{IR} - F_{2-}) \right] + 2F, \\ \theta_{24} &= -\frac{1}{2M^2} \tau(1+\tau)(F_{1+} + (\tau+2)F_d),\end{aligned}\quad (53)$$

where $S_p = S + X = 2S - Q^2$, and

$$\begin{aligned}F_d &= \frac{1}{\tau} \left(\frac{1}{\sqrt{C_2}} - \frac{1}{\sqrt{C_1}} \right), \\ F_{1+} &= \frac{1}{\sqrt{C_1}} + \frac{1}{\sqrt{C_2}},\end{aligned}$$

$$\begin{aligned}
F_{2\pm} &= m^2 \left(\frac{B_2}{C_2^{3/2}} \pm \frac{B_1}{C_1^{3/2}} \right), \\
F_{IR} &= F_{2+} - (Q^2 + 2m^2)F_d, \\
F &= \frac{1}{\sqrt{\lambda_q}}.
\end{aligned} \tag{54}$$

Here:

$$\begin{aligned}
C_1 &= 4m^2(Q^2 + \tau(Q^2 + v) - \tau^2 M^2) \\
&\quad + (Q^2 + \tau S)^2, \\
C_2 &= 4m^2(Q^2 + \tau(Q^2 + v) - \tau^2 M^2) \\
&\quad + (Q^2 + \tau(v - X))^2, \\
B_1 &= \tau(S(Q^2 + v) + 2M^2 Q^2) \\
&\quad + Q^2(S_p - v), \\
B_2 &= \tau((X - v)(Q^2 + v) - 2M^2 Q^2) \\
&\quad + Q^2(S_p - v).
\end{aligned} \tag{55}$$

As a result, we obtain

$$d\sigma_R = -\frac{\alpha^3 dQ^2 d\tau dv}{2\lambda_S(1+\tau)t^2} \sum_{i=1}^2 \sum_{j=1}^{k_i} \mathcal{F}_i(t) R^{j-2} \theta_{ij}(v, \tau, Q^2). \tag{56}$$

A straightforward integration over the photon phase space is not possible because of infrared divergence coming from the term with $j = 1$ in (52) at the point $v = 0$ (or $R = 0$). For the consistent extraction and cancellation of the infrared divergence we use the Bardin-Shumeiko approach [16]. Following this method, the identical transformation,

$$d\sigma_R = d\sigma_R - d\sigma_R^{IR} + d\sigma_R^{IR} = d\sigma_R^F + d\sigma_R^{IR}, \tag{57}$$

allows us to split $d\sigma_R$ into the infrared-free $d\sigma_R^F$ and infrared-dependent $d\sigma_R^{IR}$ parts. The last one can be obtained before integration over ϕ_k as a term factorized in front of the Born cross section:

$$d\sigma_R^{IR} = \frac{1}{R} \lim_{R \rightarrow 0} R d\sigma_R = -\frac{\alpha}{\pi^2} d\sigma_B \frac{v dv d\tau d\phi_k}{2(1+\tau)^2 \sqrt{\lambda_q}} \mathcal{F}_{IR}, \tag{58}$$

where

$$\mathcal{F}_{IR} = \frac{1}{4} \left(\frac{k_1}{kk_1} - \frac{k_2}{kk_2} \right)^2. \tag{59}$$

Note that

$$F_{IR} = \frac{R^2}{2\pi \sqrt{\lambda_q}} \int_0^{2\pi} d\phi_k \mathcal{F}_{IR}. \tag{60}$$

The treatment of the infrared divergence by the Bardin-Shumeiko approach requires to separate $d\sigma_R^{IR}$ into the soft δ_S and hard δ_H parts

$$\frac{d\sigma_R^{IR}}{dQ^2} = \frac{\alpha}{\pi} \delta_{IR} \frac{d\sigma_B}{dQ^2} = \frac{\alpha}{\pi} (\delta_S + \delta_H) \frac{d\sigma_B}{dQ^2} \tag{61}$$

by introducing of the infinitesimal inelasticity \bar{v}

$$\begin{aligned}
\delta_S &= -\frac{1}{\pi} \int_0^{\bar{v}} dv \int \frac{d^3 k}{k_0} \delta((p_1 + q - k)^2 - M^2) \mathcal{F}_{IR}, \\
\delta_H &= -\frac{1}{\pi} \int_{\bar{v}}^{v_{cut}} dv \int \frac{d^3 k}{k_0} \delta((p_1 + q - k)^2 - M^2) \mathcal{F}_{IR}.
\end{aligned} \tag{62}$$

This separation allows us to calculate δ_S in the dimensional regularization by choosing the individual reference systems for each leptonic propagator $1/kk_1$ and $1/kk_2$, as well as their combination to make them independent of the azimuthal angle ϕ_k while the hard part can be calculated in straightforward way without any regularization.

It can be seen from the explicit expressions for δ_S and δ_H – details of their calculation can be found in Appendix A – that for $Q^2 \rightarrow 0$ both of them tend to zero and their sum

$$\begin{aligned}
\delta_{IR} &= J_0 \left[P_{IR} + \log \frac{v_{cut}}{\mu M} \right] + \frac{1}{2} S L_S + \frac{1}{2} X L_X \\
&\quad + S_\phi(k_1, k_2, p_2)
\end{aligned} \tag{63}$$

does not depend on the separated inelasticity \bar{v} and contains the infrared term P_{IR} as well as a parameter μ that have to be cancelled against corresponding terms in δ_{vert} .

Therefore RC for fixed Q^2 read:

$$\frac{d\sigma_{RC}}{dQ^2} = \frac{\alpha}{\pi} (\delta_{VR} + \delta_{vac}^l) \frac{d\sigma_B}{dQ^2} + \frac{d\sigma_{AMM}}{dQ^2} + \frac{d\sigma_F}{dQ^2}. \tag{64}$$

Here the expression for δ_{vac}^l is defined in Eq. (41), δ_{VR} is an infrared-free sum δ_{vert} and δ_{IR} :

$$\begin{aligned}
\delta_{VR} &= \delta_{IR} + \delta_{vert} = J_0 \log \frac{v_{cut}}{mM} + \frac{1}{2} S L_S + \frac{1}{2} X L_X \\
&\quad + S_\phi(k_1, k_2, p_2) - 2 + \left(\frac{3}{2} Q^2 + 4m^2 \right) L_m \\
&\quad - \frac{Q^2 + 2m^2}{\sqrt{\lambda_m}} \left(\frac{1}{2} \lambda_m L_m^2 + 2 \text{Li}_2 \left[\frac{2\sqrt{\lambda_m}}{Q^2 + \sqrt{\lambda_m}} \right] \right. \\
&\quad \left. - \frac{\pi^2}{2} \right).
\end{aligned} \tag{65}$$

The general expression for $S_\phi(k_1, k_2, p_2)$ is reproduced in Appendix B and for our case

$$\begin{aligned}
S_\phi(k_1, k_2, p_2) &= \frac{Q^2 + 2m^2}{\sqrt{\lambda_m}} \left(\frac{1}{4} \lambda_X L_X^2 - \frac{1}{4} \lambda_S L_S^2 \right. \\
&\quad + \text{Li}_2 \left[1 - \frac{(X + \sqrt{\lambda_X}) \rho}{8m^2 M^2} \right] \\
&\quad + \text{Li}_2 \left[1 - \frac{\rho}{2(X + \sqrt{\lambda_X})} \right] \\
&\quad \left. - \text{Li}_2 \left[1 - \frac{Q^2 (S + \sqrt{\lambda_S}) \rho}{2M^2 (Q^2 + \sqrt{\lambda_m})^2} \right] \right)
\end{aligned}$$

$$- \text{Li}_2 \left[1 - \frac{2m^2 Q^2 \rho}{(Q^2 + \sqrt{\lambda_m})^2 (S + \sqrt{\lambda_S})} \right], \quad (66)$$

where $\rho = (Q^2 + \sqrt{\lambda_m})(S_p - \sqrt{\lambda_m})/\sqrt{\lambda_m}$.

The anomalous magnetic moment contribution is represented by Eqs. (39). At last, the finite part of the cross section reads:

$$\frac{d\sigma_F}{dQ^2} = -\frac{\alpha^3}{2\lambda_S} \int_0^{v_{cut}} dv \sum_{i=1}^2 \left[4 \frac{J_0 \theta_B^i \mathcal{F}_i(Q^2)}{vQ^4} + \int_{\tau_{min}^q}^{\tau_{max}^q} \frac{d\tau}{(1+\tau)t^2} \sum_{j=1}^{k_i} \mathcal{F}_i(t) R^{j-2} \theta_{ij}(v, \tau, Q^2) \right], \quad (67)$$

where the integration limits over τ are defined by Eqs. (22).

6 Real photon emission for fixed scattering angle

The phase space for this case reads:

$$d\Gamma_3 = J_\theta(v) \frac{v dv d\cos\theta d\tau d\phi_k}{2^8 \pi^4 (1+\tau)^2 \sqrt{\lambda_S \lambda_v}}, \quad (68)$$

where

$$J_\theta(v) = \frac{\lambda_S - vS - Q_R^2(v)(S + 2M^2)}{(S + 2M^2)^2 - \lambda_S \cos^2\theta} \times \left(\frac{S + 2M^2}{\cos\theta} + M \sqrt{\frac{\lambda_S}{\mathcal{D}}} (S - v + 2m^2) \right), \quad (69)$$

and $J_\theta(0) = j_\theta$.

After some algebra similar to the previous section, we have:

$$\frac{d\sigma_{RC}}{d\cos\theta} = \frac{\alpha}{\pi} (\delta_{VR} + \delta_{vac}^l) \frac{d\sigma_B}{d\cos\theta} + \frac{d\sigma_{AMM}}{d\cos\theta} + \frac{d\sigma_F}{d\cos\theta}, \quad (70)$$

while the finite part has the following structure:

$$\frac{d\sigma_F}{d\cos\theta} = -\frac{\alpha^3}{2\lambda_S} \int_0^{v_{cut}} dv \sum_{i=1}^2 \left[4j_\theta \frac{J_0 \theta_B^i \mathcal{F}_i(Q^2)}{vQ^4} + J_\theta(v) \times \int_{\tau_{min}^\theta}^{\tau_{max}^\theta} \frac{d\tau}{(1+\tau)t^2} \sum_{j=1}^{k_i} \mathcal{F}_i(t) R^{j-2} \theta_{ij}(v, \tau, Q_R^2(v)) \right]. \quad (71)$$

7 Numerical results

Here we present the relative RC which is defined as a ratio of RC to the Born cross section

$$\delta_{RC} = \frac{d\sigma_{RC}/d\zeta}{d\sigma_B/d\zeta} \quad (72)$$

both for fixed Q^2 ($\zeta = Q^2$) and the scattering angle ($\zeta = \cos\theta$) presented in Eqs. (64) and (70), respectively. Corresponding Born contributions are defined by Eqs. (32).

As mentioned above, a cut applied on the upper integration limit over inelasticity allows to reduce the contribution of hard photon emission. On the other hand, for the radiative process the energy of the scattering lepton depends on the inelasticity as it is presented in Eqs. (9) for the fixed Q^2 and (15) for the fixed scattering angle. Therefore instead of the upper limit over inelasticity, we can set a cut on the lower limit of the scattered-lepton energy.

The result of these cuts under MUSE kinematic conditions [11] is presented in Fig. 4. As we can see, the situation for the scattering electron for fixed Q^2 and scattering angle for soft photon emission is almost identical while for hard photon emission it is dramatically different: for the fixed scattering angle RC increase to 80% while for the fixed Q^2 RC do not exceed 5%. This is a key observation for both electron and positron scattering in the experimental analysis.

Another interesting issue consists in the ε -behavior at JLab kinematic conditions [20, 21]. Following our previous work [24] we can define

$$\varepsilon_q = \left[1 + 2 \left(1 + \frac{Q^2}{4M^2} \right) \frac{M^2(Q^2 - 2m^2)}{S(X - v_{cut}) - M^2 Q^2} \right]^{-1} \quad (73)$$

for fixed Q^2 and in a similar way

$$\varepsilon_\theta = \varepsilon_q \Big|_{Q^2 \rightarrow Q_R^2(v_{cut})} \quad (74)$$

for fixed scattering angle.

The numerical result presented in Fig. 5 shows almost identical values of RC for the soft photon emission and different behavior of RC with the hard real photons for the fixed Q^2 vs. a fixed scattering angle. In the first case with growing v_{cut} the value of the variable ε decreases and RC for the hard photon (when $v_{cut} = v_q$) does not exceed 1.6 times the Born contribution, while for the fixed scattering angle ε goes a little bit up but the absolute value of the relative RC rapidly increases reaching the values up to 45 times (when $v_{cut} = v_\theta$). Such a rapid change of RC near the kinematic limit of fixed-angle measurements sets more stringent requirements on energy resolution for lepton detection in the fixed-angle kinematic setting, as opposed to fixed Q^2 analysis.

8 Conclusion

We discussed essential differences between the kinematic description of radiative effects for fixed Q^2 vs.

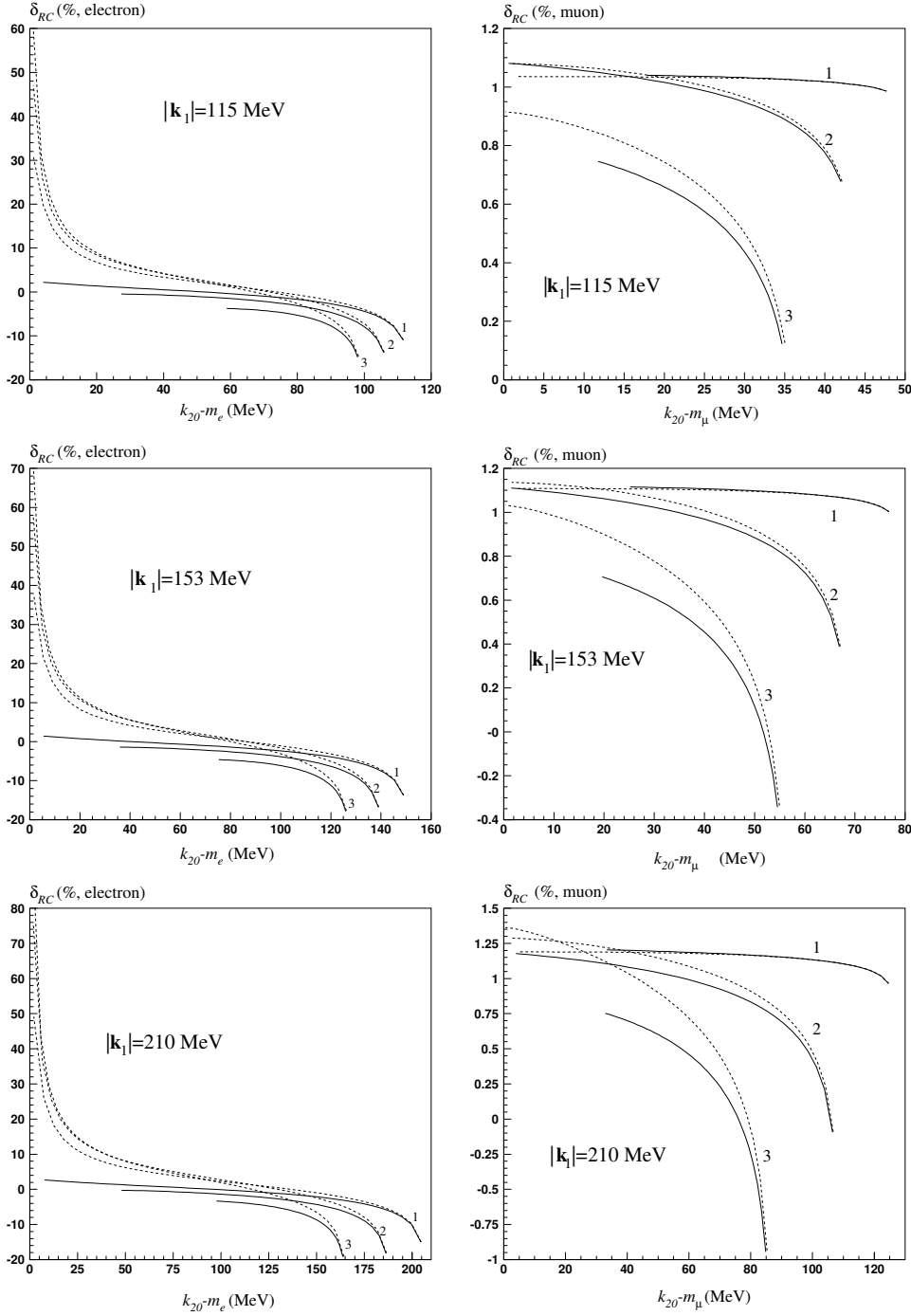


Fig. 4 Relative RC vs the value of the scattering lepton kinetic energy for elastic ep and μp scattering, beam momenta is equal to 115 MeV, 153 MeV and 210 MeV for $\theta = 20^\circ$ (1), 60° (2), 100° (3). Solid (dashed) line corresponds to fixed Q^2 ($\cos\theta$).

fixed scattering angle in the elastic lepton-proton scattering. In particular, it was shown that for the description of hard-photon emission at fixed scattering angle, even for the high-energy electron-proton scattering the ultrarelativistic approximation is not applicable in the considered kinematics as we approach the limits of

phase space. The technique of Bardin-Shumeiko for the covariant extraction and cancellation of the infrared divergence as well as the explicit expressions for RC to the lepton current in unpolarized elastic lp -scattering within these two cases were presented. The numerical analysis within kinematic conditions of Jefferson Lab

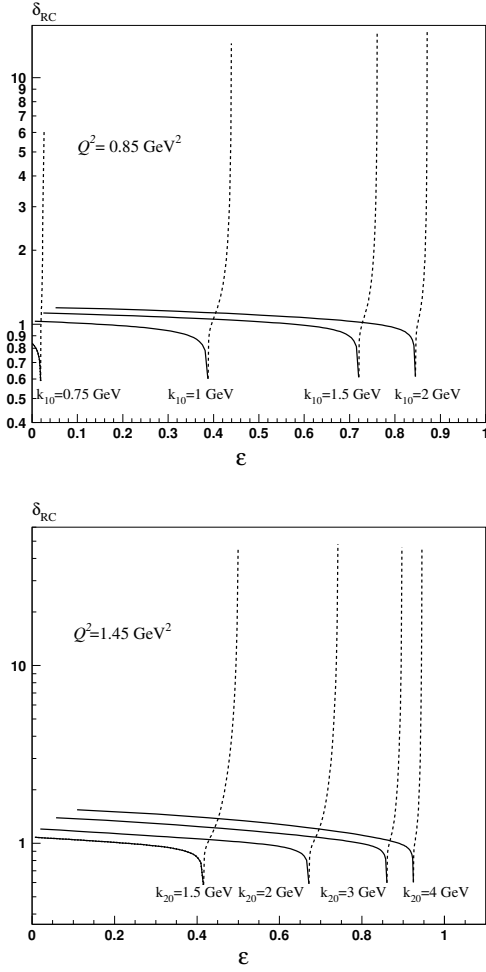


Fig. 5 Relative RC vs value of the scattering particle kinetic energy as a function of ε at $Q^2 = 0.85 \text{ GeV}^2$ and $Q^2 = 1.45 \text{ GeV}^2$. The solid (dashed) correspond fixed Q^2 ($\cos\theta$).

measurements and MUSE experiment in PSI has shown the almost identical values of RC for the soft photon emission and significantly different behavior of RC with the hard real photon for the fixed Q^2 compared with fixing a lepton scattering angle. The presented formalism may be of use also for the high-energy muon scattering case of the AMBER proposal [25].

Based on our recent work [24], in the nearest future we intend to generalize the numerical comparison of RC calculation for the fixed Q^2 and scattering angle with an electron/positron and muon/antimuon charge asymmetry. We also intend to include simulations of radiative events for the fixed scattering angle into Monte Carlo generator ELRADGEN [26,27], that is used for the hard photon generation in the elastic lp -scattering.

Acknowledgements The authors thank the anonymous referee of this paper for insightful comments.

Data Availability Statement This manuscript has no associated data or the data will not be deposited. [Authors' comment: The discussion presented in this article develops from already existing and published data which are duly referenced.]

Appendix A: Calculation of δ_S and δ_H

For calculation of δ_S in the dimensional regularization

$$\begin{aligned} \frac{d^3 k'}{k'_0} &\rightarrow \frac{d^{n-1} k'}{(2\pi\mu)^{n-4} k_0} \\ &= \frac{2\pi^{n/2-1} k_0^{n-3} dk_0 (1-x^2)^{n/2-2} dx}{(2\pi\mu)^{n-4} \Gamma(n/2-1)}, \end{aligned} \quad (\text{A.1})$$

where $x = \cos\theta$ (θ is defined as the spatial angle between the photon three-momentum and \mathbf{k}'_i ($i = 1-3$) that are introduced below) and μ is an arbitrary parameter of the dimension of a mass the reference system $\mathbf{p}_1 + \mathbf{q} = \mathbf{0}$ is used.

The Feynman parameterization of (59) gives

$$\begin{aligned} \mathcal{F}_{\mathcal{IR}} &= \frac{1}{4k_0'^2} \int_0^1 dy \left[\frac{m^2}{k_{10}'^2 (1-x\beta_1)^2} + \frac{m^2}{k_{20}'^2 (1-x\beta_2)^2} \right. \\ &\quad \left. - \frac{Q^2 + 2m^2}{k_{30}'^2 (1-x\beta_3)^2} \right] = \frac{1}{4k_0'^2} \int_0^1 dy \mathcal{F}(x, y). \end{aligned} \quad (\text{A.2})$$

Here $\beta_i = |\mathbf{k}'_i|/k'_0$ for $i = 1, 2, 3$ and $k_3 = yk_1 + (1-y)k_2$.

After the substitution of Eqs. (A.1) and (A.2) into the definition of δ_S by Eq. (62) and, using δ -function, integrated over the photon energy k_0 one can find that

$$\begin{aligned} \delta_S &= -\frac{1}{2(4\mu\sqrt{\pi})^{n-4} \Gamma(n/2-2)} \int_{-1}^1 dx (1-x^2)^{n/2-2} \\ &\quad \times \int_0^1 dy \mathcal{F}(x, y) \int_0^{\bar{v}} \frac{dv}{v} \left(\frac{v}{M} \right)^{n-4}. \end{aligned} \quad (\text{A.3})$$

The integration over v and the expansion of the obtained expression into the Laurent series around $n = 4$ result in

$$\delta_S = \delta_S^{IR} + \delta_S^1, \quad (\text{A.4})$$

where

$$\delta_S^{IR} = -\frac{1}{2} \left[P_{IR} + \log \frac{\bar{v}}{\mu M} \right] \int_0^1 dy \int_{-1}^1 dx \mathcal{F}(x, y) \quad (\text{A.5})$$

and

$$\delta_S^1 = -\frac{1}{4} \int_0^1 dy \int_{-1}^1 dx \log \left[\frac{1}{4} (1-x^2) \right] \mathcal{F}(x, y). \quad (\text{A.6})$$

Here P_{IR} is the infrared divergent term defined by Eq. (43). Taking into account that $k_3^2 = y(1-y)Q^2 + m^2$ the integration over x and y variables in δ_S^{IR} is simple:

$$\delta_S^{IR} = J_0 \left[P_{IR} + \log \frac{\bar{v}}{\mu M} \right], \quad (\text{A.7})$$

where J_0 is defined by Eq. (42).

For the calculation of δ_S^1 we note that in the system $\mathbf{p}_1 + \mathbf{q} = \mathbf{0}$ the energies of the initial and scattering lepton through the invariants:

$$k'_{10} = \frac{X}{2M^2}, \quad k'_{20} = \frac{S}{2M^2}. \quad (\text{A.8})$$

As a result,

$$\delta_S^1 = \frac{1}{2}SL_S + \frac{1}{2}XL_X + S_\phi(k_1, k_2, p_2), \quad (\text{A.9})$$

where

$$L_S = \frac{1}{\sqrt{\lambda_S}} \log \frac{S + \sqrt{\lambda_S}}{S - \sqrt{\lambda_S}},$$

$$L_X = \frac{1}{\sqrt{\lambda_X}} \log \frac{X + \sqrt{\lambda_X}}{X - \sqrt{\lambda_X}}, \quad (\text{A.10})$$

and

$$S_\phi(k_1, k_2, p_2) = \frac{Q^2 + 2m^2}{4} \int_{-1}^1 dx \int_0^1 dy \frac{\log[(1-x^2)/4]}{k_{30}'^2 (1-x\beta_3)^2}. \quad (\text{A.11})$$

Notice that the standard expressions for S_ϕ are rather cumbersome, see for example Eqs. (35) and (A.14) of work [17]. In Appendix B we present a more compact analytical expression for this quantity.

For the calculation of δ_H the straightforward integration is used. Taking into account (60), one can find that

$$\delta_H = - \int_{\bar{v}}^{v_{cut}} \frac{dv}{v} \int_{\tau_{min}}^{\tau_{max}} d\tau F_{IR} = J_0 \log \frac{v_{cut}}{\bar{v}}. \quad (\text{A.12})$$

Appendix B: Calculation of S_ϕ

Here we present a general approach suggested by 't Hooft and Veltman in their work [28] for a compact representation of the S_ϕ -function introduced by Bardin and Shumeiko in [16]. Let us consider a real photon with a momentum k and three other time-like four-momenta a_i ($i = 1, 2, 3$) with masses $m_i^2 = a_i^2$. The basic idea consists in Feynman parameterization. Instead of usual approach used in the standard Bardin-Shumeiko technique with two fermionic propagator presented in previous appendix, taken in the system $\mathbf{a}_3 = 0$:

$$\frac{1}{a_1 k} \frac{1}{a_2 k} = \gamma \frac{1}{a_1 k} \frac{1}{\gamma a_2 k} = \frac{\gamma}{k_0^2} \int_0^1 \frac{dy}{a_{40}^2 (1-x\beta)^2}. \quad (\text{B.13})$$

Here, as in the previous appendix $x = \cos \theta$, a new four-vector $a_4 = ya_1 + (1-y)\gamma a_2$, and $\beta = |\mathbf{a}_4|/a_{40}$. The quantity γ is choosing in such a way, that $(a_1 - \gamma a_2)^2 = 0$, i.e. $a_1 - \gamma a_2$ is lightlike vector.

Now introduce the following invariants:

$$s_1 = 2a_1 a_3, \quad \lambda_1 = s_1^2 - 4m_1^2 m_3^2,$$

$$s_2 = 2a_2 a_3, \quad \lambda_2 = s_2^2 - 4m_2^2 m_3^2,$$

$$s_3 = 2a_1 a_2, \quad \lambda_3 = s_3^2 - 4m_1^2 m_2^2. \quad (\text{B.14})$$

Then equation $(a_1 - \gamma a_2)^2 = 0$ has the following two solutions:

$$\gamma_1 = \frac{2m_1^2}{s_3 + \sqrt{\lambda_3}}, \quad \gamma_2 = \frac{s_3 + \sqrt{\lambda_3}}{2m_2^2}, \quad (\text{B.15})$$

and the generalized form of S_ϕ looks as (A.11):

$$S_\phi = \frac{1}{4} \gamma s_3 \int_0^1 \frac{dy}{a_{40}^2} \int_{-1}^1 dx \frac{\log[(1-x^2)/4]}{(1-x\beta)^2}. \quad (\text{B.16})$$

The first integration over x is straightforward

$$S_\phi = \frac{1}{2} \gamma s_3 \int_0^1 \frac{dy}{m_4^2 \beta} \log \frac{1-\beta}{1+\beta}, \quad (\text{B.17})$$

where $m_4^2 = a_4^2 = ym_1^2 + (1-y)\gamma^2 m_2^2$. The second integration has to be performed after the standard substitutions, while taking into account that for the first two momenta $a_{i0} = s_i/(2m_3)$.

Finally, we can find that for the general case S_ϕ depends on six variables and for $\gamma = \gamma_1$ it has the following structure:

$$S_\phi(a_1, a_2, a_3) = \frac{s_3}{\sqrt{\lambda_3}} \left(\log^2 \frac{s_1 + \sqrt{\lambda_1}}{2m_1 m_3} - \log^2 \frac{s_2 + \sqrt{\lambda_2}}{2m_2 m_3} \right. \\ \left. + \text{Li}_2 \left[1 - \frac{(s_1 + \sqrt{\lambda_1})\rho}{8m_1^2 m_3^2} \right] \right. \\ \left. + \text{Li}_2 \left[1 - \frac{\rho}{2(s_1 + \sqrt{\lambda_1})} \right] \right. \\ \left. - \text{Li}_2 \left[1 - \frac{(s_2 + \sqrt{\lambda_2})\rho}{4m_2^2 (s_3 + \sqrt{\lambda_3})} \right] \right. \\ \left. - \text{Li}_2 \left[1 - \frac{m_2^2 \rho}{(s_2 + \sqrt{\lambda_2})(s_3 + \sqrt{\lambda_3})} \right] \right), \quad (\text{B.18})$$

where $\rho = (2s_1(s_3 + \sqrt{\lambda_3}) - 4m_1^2 s_2)/\sqrt{\lambda_3}$.

It should be noted that

$$S_\phi(a_1, a_2, a_3) = S_\phi(a_2, a_1, a_3) \quad (\text{B.19})$$

The r.h.s. of this equation corresponds $\gamma = \gamma_2$.

In our case $a_1 = k_1$, $a_2 = k_2$, $a_3 = p_2$, and $s_1 = X$, $s_2 = S$, $s_3 = Q^2 + 2m^2$, $m_1 = m_2 = m$, $m_3 = M$.

References

1. L. Andivahis et al. Phys. Rev. D **50**, 5491 (1994)
2. I. A. Qattan et al. Phys. Rev. Lett. **94**, 142301 (2005)
3. M. K. Jones et al. (Jefferson Lab Hall A), Phys. Rev. Lett. **84**, 1398 (2000)
4. O. Gayou et al. (Jefferson Lab Hall A), Phys. Rev. Lett. **88**, 092301 (2002)
5. P. J. Mohr, B. N. Taylor and D. B. Newell, Rev. Mod. Phys. **80**, 633 (2008)
6. I. Sick, Phys. Lett. B **576**, 62 (2003)
7. R. Pohl, et al., Nature **466**, 213 (2010)
8. W. Xiong, et al., Nature **575**, 147 (2019)
9. A. Accardi, et al., Eur. Phys. J. A **57**, 8 (2021)
10. A. Afanasev, P. G. Blunden, D. Hasell and B. A. Raue, Prog. Part. Nucl. Phys. **95**, 245-278 (2017)
11. R. Gilman et al. (MUSE), arXiv:1709.09753
12. A. Gasparian et al. (PRad), arXiv:2009.10510
13. N. Kaiser, J. Phys. G **37**, 115005 (2010)
14. M. Vanderhaeghen et al., Phys. Rev. C **62**, 025501 (2000)
15. L. W. Mo and Y. S. Tsai, Rev. Mod. Phys. **41**, 205 (1969).
16. D. Y. Bardin and N. M. Shumeiko, Nucl. Phys. B **127**, 242 (1977)

17. I. Akushevich, H. Gao, A. Ilyichev and M. Meziane, Eur. Phys. J. A **51**, 1 (2015)
18. R. D. Bucoveanu and H. Spiesberger, Eur. Phys. J. A **55**, 57 (2019)
19. P. Banerjee, T. Engel, A. Signer and Y. Ulrich, SciPost Phys. **9**, 027 (2020)
20. D. Adikaram et al. (CLAS), Phys. Rev. Lett. **114**, 062003 (2015)
21. D. Rimal et al. (CLAS), Phys. Rev. C **95**, no.6, 065201 (2017)
22. A. Afanasev, I. Akushevich and N. Merenkov, Phys. Rev. D **64**, 113009 (2001)
23. I. Akushevich and A. Ilyichev, Phys. Rev. D **100**, no.3, 033005 (2019)
24. A. Afanasev and A. Ilyichev, arXiv:2007.02087
25. B. Adams et al. (COMPASS++/AMBER), CERN-SPSC-2019-022, SPSC-P-360, <http://cds.cern.ch/record/2676885>
26. A. V. Afanasev, I. Akushevich, A. Ilyichev and B. Niczyporuk, Czech. J. Phys. **53**, B449-B454 (2003) arXiv:hep-ph/0308106
27. I. Akushevich, O. F. Filoti, A. N. Ilyichev and N. Shumeiko, Comput. Phys. Commun. **183**, 1448-1467 (2012)
28. G. 't Hooft and M. J. G. Veltman, Nucl. Phys. B **153**, 365-401 (1979)